Ceramics-Silikáty 63 (1), 124-130 (2019)
www.ceramics-silikaty.cz doi: 10.13168/cs.2019.0004

ELECTROPHORETIC DEPOSITION OF $BiVO_4$ LAYERS ON FTO SUBSTRATES FOR PHOTO ELECTRO-CHEMICAL CELLS

#C. MEGNIN*, M. MAUCK*, **, D. HERTKORN*, **, T. HANEMANN*, ***, C. MUELLER**

*University of Freiburg, Department of Microsystems Engineering (IMTEK), Laboratory for Materials Processing, 79110 Freiburg, Germany
**University of Freiburg, Department of Microsystems Engineering (IMTEK), Laboratory for Process Technology, 79110 Freiburg, Germany
***Karlsruhe Institute of Technology (KIT), Institute of Applied Materials (IAM), 76344 Eggenstein-Leopoldshafen, Germany

#E-mail: c.megnin@gmx.de

Submitted October 8, 2018; accepted January 12, 2019

Keywords: Solar water splitting, Photo electro-chemical (PEC) cells, $BiVO_4$, External quantum efficiency (EQE)

In this paper the deposition of $BiVO_4$ onto fluorine doped tin oxide (FTO) substrates by electrophoretic deposition (EPD) is presented. The $BiVO_4$ powder was fabricated by a mixed oxide route and added by a solvent and dispersant to achieve the suspension for EPD. The particle size, sintering parameters, and crystal structure of the powder were characterized by laser light diffraction, dilatometer, and X-ray diffraction, respectively. EPD was performed at deposition voltages between 12.5 V and 100 V resulting in layer thicknesses in the range of 0.5 µm and 2.8 µm after sintering. The current density of the layers was determined for frontside and backside illumination of the FTO substrates at different wavelengths in the range between 400 nm and 600 nm. The band gap was determined at 515 nm, which corresponds to 2.5 eV. The maximum external quantum efficiency (EQE) was measured at 440 nm and backside illumination.

INTRODUCTION

The energy consumption of the global population is rising from day to day and thereby the total amount of primary energy sources is steadily decreasing [1]. A possible alternative solution for the future may be renewable energy sources. Beside solar [2], wind [3], and water [4] as renewable energy, photo electro-chemical (PEC) cells are receiving more and more interest.

PECs consist of a photo sensitive semiconductor anode and a metallic cathode within a liquid electrolyte [5, 6]. Irradiation of the anode by electromagnetic radiation results in an electrolysis of water (H_2O) to oxygen (O_2) and hydrogen (H_2) at the anode and cathode, respectively [7]. One approach of PECs is the storage of H_2, due to the geometrical separation of H_2 and O_2. The storage can be realized, for instance, within a metal hydride [8], which enables the functionality as a secondary battery for mobile applications [9, 10]. The advantage of H_2 as storage medium is the high energy density compared to other storage technologies such as electric capacitors or pressurerized fluids [11].

In the year 1972 the first PEC was presented by Honda et al. [12]. The anode consisted of a n-doped TiO_2, the cathode of platinum, and as electrolyte 1 M KOH was used. The electrolysis of H_2O was realized under illumination in combination with an external bias voltage. Subsequently other semiconductors like $SrTiO_3$ [13] or Fe_2O_3 [14] were investigated as anode materials. As material for the cathode, nickel (Ni) or platinum (Pt) was used. Due to the large band gap of TiO_2 (3.0 eV), $SrTiO_3$ (3.2 eV), and Fe_2O_3 (3.0 eV), these PECs can only be used at wavelengths below 400 nm without an external bias potential. Materials that can be used below this threshold are $BiVO_4$ and $InVO_4$ with a band gap of 2.4 eV (530 nm) and 1.9 eV (650 nm), respectively [15, 16]. The deposition of $BiVO_4$ is mostly performed by two different approaches. (1) The first is based on nano-scaled $BiVO_4$ powders, which are dispersed in an electrolyte. (2) The second approach is the deposition of a thin layer onto the cathode, which enables the separation of the gases directly. The materials can be deposited for instance by sputtering [17], sol-gel method [18], or electrophoretic deposition (EPD) [19, 20].

In this investigation, $BiVO_4$ layers are realized by EPD method onto fluorine doped tin oxide (FTO) substrates. By using this deposition method, layers with a high surface area could be achieved directly on the cathode, which combines the above mentioned advantages. In previous work the deposition of $SrTiO_3$ by EPD on nickel substrates was already shown [21]. Depending on the fabrication process of the layers, external

quantum efficiencies (EQE) more than 60 % were realized. Beside the already mentioned advantages, EPD is a fast, inexpensive and easy method, which offers the possibility to deposit layers with a wide variation of thickness. Due to the usage of nanopowders, a large interface area could be realized between the $BiVO_4$ and the electrolyte. FTO substrates are electrical conductive and transparent for visible light and, thus, enable an irradiation of the photo active layer from the frontside as well as the backside.

In this paper the operation principle of EPD and PEC, the fabrication of the powder and $BiVO_4$ layers, as well as the characterization are presented. The results are discussed with respect to the illumination orientation, the chemical behavior of the reactions, the thickness of the layers, and the illumination wavelength to increase the EQE.

EXPERIMENTAL

Operation principle

Electrophoretic Deposition

The electrophoretic deposition enables the migration of charged colloidal particles under the influence of an electric field and their deposition onto an electrode. For EPD a homogeneous liquid suspension is necessary, which consists in general of a dispersion medium, a dispersant, and the particles. The particles must be charged on the surface and can be made of polymers, pigments, dyes, ceramics, as well as metals. Two electrodes are dipped into the suspension and an electrical field is applied. This initializes the migration and deposition of the charged particles onto the corresponding electrode. The deposited mass can be calculated by the Hamaker Equation 1 [22], which is given in 1. This equation describes the deposited mass depending on the applied time and voltage.

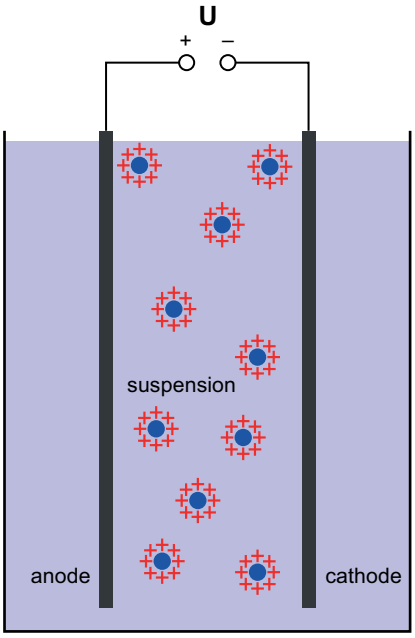

Figure 1. Schematic side view of a electrophoretic deposition (EPD) setup.

$$m(t, U) = \frac{A \cdot c \cdot \zeta \cdot \varepsilon}{d^2 \cdot \eta} \cdot t \cdot U \qquad (1)$$

The parameter A indicates the working area, c the solid concentration, ζ the Zeta potential, ε the dielectric constant, d the distance between the electrodes, and η the viscosity of the suspension. A schematic of an electrophoretic deposition setup is shown in Figure 1.

Photo Electro-Chemical Cell

Figure 2 shows a schematic side view of our PEC. It consists of a $BiVO_4$ layer on a FTO substrate as anode. The FTO substrate is covered by a silicone mask on both sides. The hole stack is dipped into KOH as electrolyte. A platinum coated nickel foam is used as counter electrode. By illumination of the $BiVO_4$ layer with LED light with suitable wavelength, H_2O is splitted into oxygen (O_2) and hydrogen (H_2). At the same time, free electrons are generated. The resulting current is measured by an amperemeter, which is an indicator for the generated charge carriers.

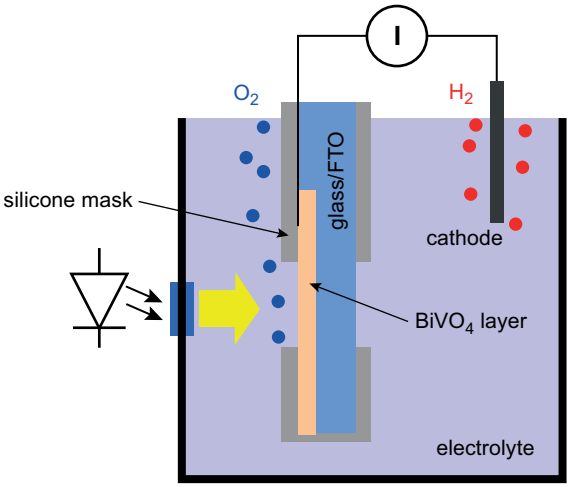

Figure 2. Schematic side view of a photo electro-chemical (PEC) cell setup.

RESULTS AND DISCUSSION

Fabrication of $BiVO_4$ layer

Powder Preparation

In this investigation, $BiVO_4$ powder was produced by a solid state mixed oxide reaction. The chemical reaction is shown in Equation 2. The two educt powders Bi_2O_3 (Alfa Aesar, 99.5 %) and V_2O_5 (Alfa Aesar, 99.6 %) were mixed with the correct molar proportions before reaction. Subsequently the mixture was homogenized by wet milling in 2-propanol and calcinated in a furnace in

ambient air for 48 h at 800 °C. The heating and cooling rate was 5 K·min^{-1}. The resulting coarse $BiVO_4$ granulate was crushed by wet milling in a planetary mill (Retsch PM400) for 4 h, followed by a drying step.

$$Bi_2O_3 + V_2O_5 \rightarrow 2\ BiVO_4 \quad (2)$$

Suspension preparation

Before EPD deposition process, the $BiVO_4$ powder has to be dispersed. The corresponding suspension contains $BiVO_4$ powder, 2-propanol, and an organic dispersant. At first the dispersant (trioxadecanoic acid) plus 2-propanol were mixed and stirred magnetically for 5 min. Then the $BiVO_4$ powder was continuously added into the solution and stirred for further 10 min. To crush agglomerated particles and to achieve a homogeneous suspension, the mixture was ultrasonified (Sonifier W450, Branson) for 3 min.

Electrophoretic deposition and sintering

The suspension was deposited onto FTO substrates with dimensions of 10 × 17 mm^2, which were diced and cleaned with acetone and 2-propanol in an ultrasonic bath. In a last step the working area of 10 × 10 mm^2 was defined by masking. The substrates were positioned parallel to a platinum counter electrode and dipped into the suspension by a stepping motor. For the deposition, voltages of 12.5, 25, 50, and 100 V were applied for 6 s. After deposition, the substrate was removed vertically out of the suspension with a velocity of 1 mm·s^{-1} and dried at ambient conditions.

The resulting layers were sintered in a furnace (CWF 1300, Carbolite) for 1 hour at 650 °C with a heating and cooling rate of 5 K·min^{-1}.

Characterization of $BiVO_4$ layer

The particle size distribution (PSD) of the $BiVO_4$ powder was determined by laser light diffraction (Beckman Coulter LS 230). In Figure 3 the time dependent particle size of the powder during the milling process is shown. After 4 h of milling, the d_{50} is 200 nm and the d_{90} is 750 nm. These particle sizes enable the deposition of samples with thicknesses of a few micrometers. Furthermore, the nanosized particles favour a high surface area of the anode, which increases the reactivity and decreases the sintering temperature.

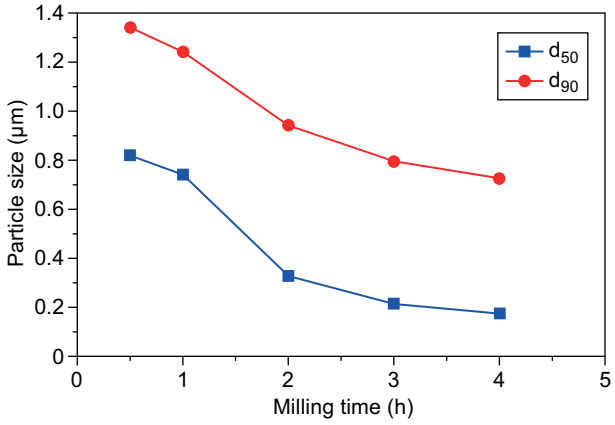

Figure 3. Time dependent particle sizes (d_{50} and d_{90}) during milling.

Dilatometer measurements (Netsch 420C) of the $BiVO_4$ were carried out to find the sintering parameters. Pellets with a diameter of 6 mm and a length of 10 mm were pressed and sintered at temperatures up to 700 °C with a heating and cooling rate of 5 K·min^{-1} in ambient air. In Figure 4 the results are shown. The sintering process took place in a temperature range between 500 °C and 600 °C. To get a sufficient adhesion to the FTO substrate, the sintering temperature was set to 650 °C.

The crystal structure was determined by XRD (Bruker D5000). Figure 5 shows the a XRD measurement of the powder and the deposited layer. The peaks, which match to the monoclinic $BiVO_4$ are marked

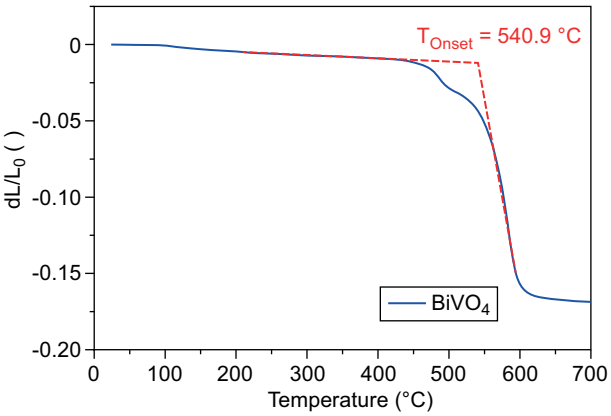

Figure 4. Dilatometer measurement of $BiVO_4$ powder.

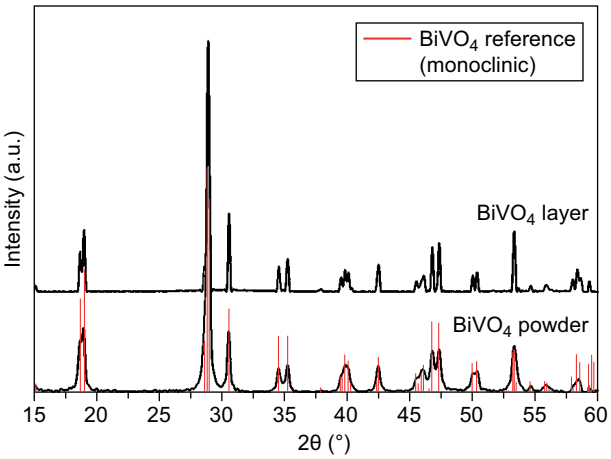

Figure 5. XRD measurement of $BiVO_4$ powder and deposited layer as well as the reference structure of the monoclinic phase (marked in hatched line).

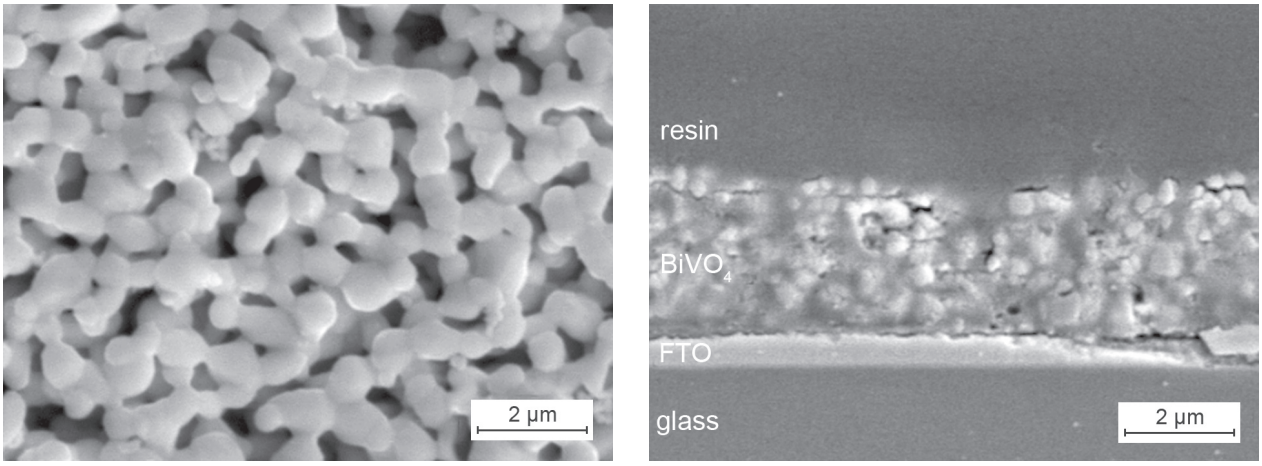

a) b)

Figure 6. SEM images of sintered $BiVO_4$ layers.

in hatched line. The peaks of the deposited layer are narrower compared to the powder sample, due to the sintering process and the corresponding grain growth.

SEM images (Zeiss DSM 962) are made to analyze the morphology and the thickness of the layers. For measuring the thickness, the samples have been embedded into a polymer structure to investigate the side view. Figure 6 shows a top view and a side view SEM image of a sintered $BiVO_4$ layer.

The average grain size is about 1 µm and the surface structure indicates a high porosity, which applies to all deposited layers with different thicknesses. The high porosity involves a large surface area and in addition a large interface between the $BiVO_4$ and the electrolyte. In Figure 6b a cross section of the deposited $BiVO_4$ on a FTO substrate is shown. To measure the thickness of the layers, depending on the deposition voltage, the samples cross sections were taken into account. Figure 7 shows the layer thicknesses for different deposition voltages and a deposition time of 6 s each. The results follow the experimental prediction of Hamaker.

Photo electro-chemical cell

The photo current densities were measured in a two electrode setup by illuminating the $BiVO_4$ on the FTO substrates from the frontside and the backside. As optical source a LED with a wavelength of 440 nm was applied. As electrolyte, potassium hydroxide with a concentration of 1 $mol \cdot l^{-1}$ was used. In Figure 8 the current density with frontside and backside illumination is shown. In both cases, the light was switched on for 60 s and the current density was recorded simultaneously.

The higher current density with backside illumination is given by the band model of a semiconductor. The electron-hole pairs are generated within the penetration depth of light, which is about 100 nm. Starting from this point the electrons or holes have to travel different path length depending on the illumination side. Due to the higher mobility of the holes, the current density is higher with the backside illumination [19]. The reason for the different mobilities are given by the electronic and crystal structure of the $BiVO_4$. The conducting band of $BiVO_4$ mainly consists of V-3d orbitals and the

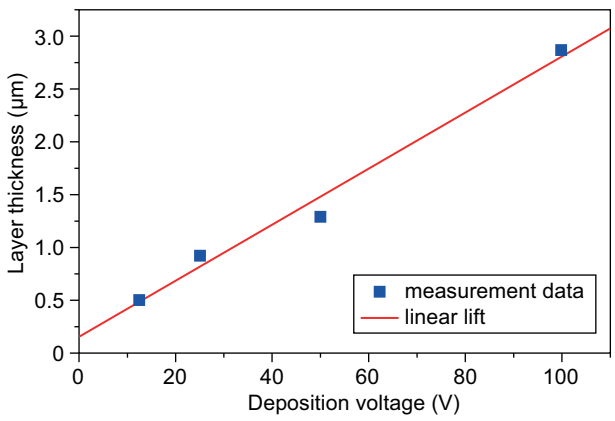

Figure 7. Measured thickness of $BiVO_4$ layers depending on the applied depostion voltage for a deposition time of 6 s.

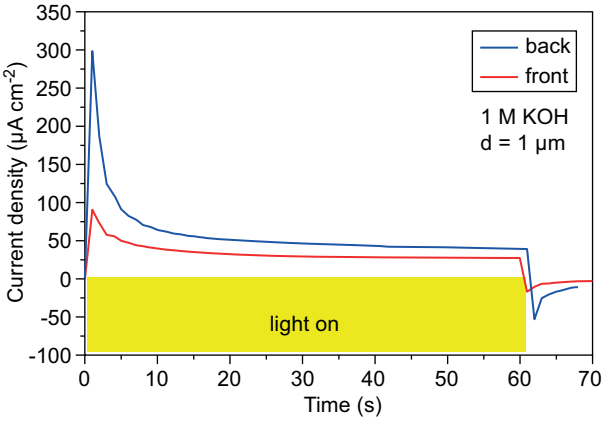

Figure 8. Photo current density of a 1 µm thick $BiVO_4$ layer on FTO substrates by front or backside illumination at 440 nm for 60 s in KOH as electrolyte.

VO_4-tetrahedra are not connected to each other within the crystal structure [23, 24]. This results in a poor electron mobility.

Furthermore the current density drops immediately after illumination, following an almost constant value. This behavior is due to the oxygen evolution reaction (OER) at the anode (Equation 3).

$$4\ OH^- + 4\ h^+ \rightarrow O_2 + 2\ H_2O \quad (3)$$

This reaction needs four holes and consists of four subreactions, which are

$$OH^* + OH^- + h^+ \rightarrow [HO^*OH] \quad (4)$$

$$[HO^*OH] \rightarrow HO^*OH \quad (5)$$

$$HO^*OH + OH^- + h^+ \rightarrow O^*OH + H_2O \quad (6)$$

$$2\ O^*OH \rightarrow 2\ OH^* + O_2 \quad (7)$$

whereby the asterisk represents a binding site at the anode surface [25].

In the first step (Equation 4) an unstable surface bonded hydrogen peroxide species is created, which in the second step (Equation 5) is converted into more stable species. This is a very critical step since the lifetime of the unstable hydrogen peroxide species is very short and could hinder significantly the complete OER. To identify if the second step is the limiting reaction, H_2O_2 was added excessively to the electrolyte to bypass Equation 4 and Equation 5. Figure 9 shows the photo current density at backside illumination with and without additional H_2O_2. By adding H_2O_2 the drop of the current density after starting the illumination is almost eliminated and the resulting value is consequently higher. From this result the limitation of the OER is found to be Equation 5.

Another parameter that influences the current density is the thickness of the $BiVO_4$ layers. Figure 10 shows the current density depending on the layer thicknesses. The current density was measured in 1 M KOH.

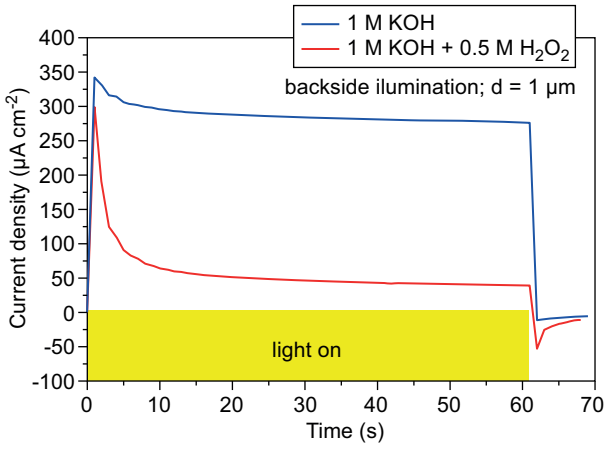

Figure 9. Photo current density of a 1 µm thick $BiVO_4$ layer on FTO substrates by backside illumination at 440 nm for 60 s with and without adding H_2O_2 to the electrolyte.

To overcome the fast dropping of the current, the measurement was made after 60 s. The current density for thinner layers is higher, due to the shorter path length of the charge carriers, which is about 70 nm [26]. The maximum current density of more than 280 µA·cm^{-2} was measured for a thickness of 1 µm.

$$EQE(\lambda) = \frac{n_{elec}}{n_{phot}} = \frac{I \cdot H \cdot c}{P \cdot \lambda \cdot q} \quad (8)$$

In order to get comparable results from different LEDs with different power, the external quantum n_{phot} to the generated charge carriers n_{elec}. I indicates the measured current density, h the Plank's constant, c the speed of light, P the measured light power, λ the wavelength of the light, and q the elementary charge.

The deposited $BiVO_4$ layers were illuminated with different wavelengths to identify the absorption edge. In Figure 11 the external quantum efficiencies with different wavelengths are shown. Below a wavelength of 515 nm the EQE raises, showing a maximum at about 440 nm. This value corresponds to a band gap of 2.5 eV, which is very similar to 2.4 eV that is found in literature [17, 23, 27].

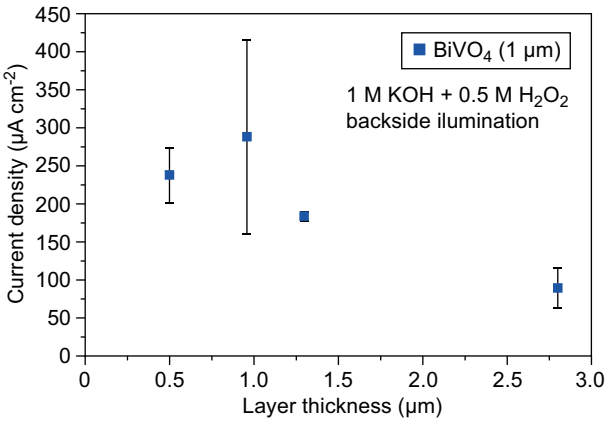

Figure 10. Photo current density for different thicknesses of $BiVO_4$ layers on FTO substrates by backside illumination at 440 nm.

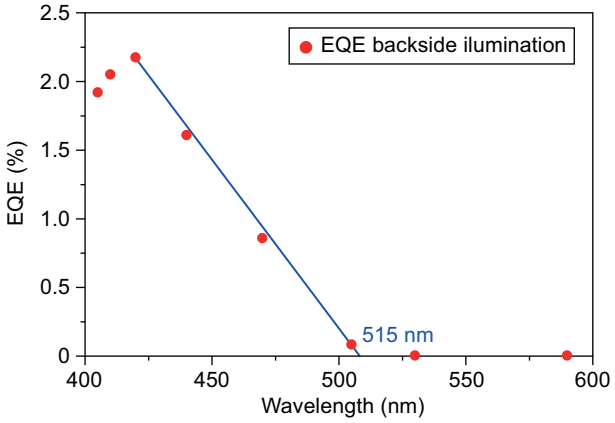

Figure 11. External quantum efficiencies (EQE) for different wavelengths by back side illumination.

In comparison to the previous work [28] of our group concerning the EQE of $SrTiO_3$, the maximum of the EQE for $BiVO_4$ is at 425 nm and hence shifted to a wavelength within the visible light. The EQE is 2.2 % compared to 64.2 % of $SrTiO_3$. In the literature an EQE of 9.0 % can be achieved with pure $BiVO_4$ for a wavelength of 350 nm [29]. By addition of FeOOH as catalyst the OER increased to 56.0 % at a wavelength of 410 nm.

CONCLUSION

This paper presents a PEC consisting of a $BiVO_4$ layer on a FTO substrate as anode and platinum as cathode within KOH as electrolyte. The FTO is covered by a silicone mask on both sides to define certain areas that are illuminated by LEDs either on the frontside or the backside. In case of illumination from the backside the measured current density is higher compared to the front side, due to the reduced path length and the higher mobility of the holes compared to the electrons. The drop of the current density after a few seconds of illumination is explained by an absence of H_2O_2, which hampers one of the subreactions of the oxygen evolution reaction. By adding H_2O_2 to the electrolyte the drop was reduced significantly and the current density showed an almost constant value of 280 $\mu A \cdot cm^{-2}$. The thickness of the $BiVO_4$ layers also influenced the current density. Thinner layers showed a higher photo current density, which is due to the shorter path length of the charge carrier. The external quantum efficiency was 2.2 % with a wavelength of 440 nm and the absorption gap was measured to be 515 nm, which corresponds to a band gap of 2.5 eV. The optimal layer thickness is 1 µm for a wavelength of 440 nm at back illumination with a resulting current density of 280 $\mu A \cdot cm^{-2}$ and an external quantum efficiency of 2.2 %.

To improve the performance of the $BiVO_4$ layers the limited electron mobility must be overcome by either decreasing of the active layer thickness or the addition of a dopant like tungsten which increases the electron mobility. Furthermore catalyst materials must be applied to prevent the limiting subreaction of the OER.

Acknowledgment

The authors would like to thank the German Research Foundation (DFG – Deutsche Forschungsgemeinschaft) for their financial support within the graduate school "Micro Energy Harvesting" (GRK 1322/2). The article processing charge was funded by the German Research Foundation (DFG) and the University of Freiburg in the funding program Open Access Publishing

REFERENCES

1. Trenberth K. E., Fasullo J. T., Kiehl J. (2009): Earth's global energy budget. Bulletin of the American Meteorological Society, 90(3), 311-324. doi: 10.1175/2008BAMS2634.1
2. Parida B., Iniyan S., Goic R. (2011): A review of solar photovoltaic technologies. Renewable and Sustainable Energy Reviews, 15, 1625–1636. doi: 10.1016/j.rser.2010.11.032
3. Kaldellis J., Zafirakis D. (2011): The wind energy (r)evolution: A short review of a long history. Renewable Energy, 36, 1887–1901. doi: 10.1016/j.renene.2011.01.002
4. Sipahutar R., Bernas S., Imanuddin M. (2013): Renewable energy and hydropower utilization tendency worldwide. Renewable and Sustainable Energy Reviews, 17, 213–215, 2013. doi: 10.1016/j.rser.2012.09.010
5. Walter M., Warren E., McKone J., Boettcher S., Mi Q., Santori E., Lewis N. (2010): Solar water splitting cells. Chemical Reviews, 110, 6446–6473. doi: 10.1021/cr1002326
6. Kudo A., Miseki Y. (2009): Heterogeneous photocatalyst materials for water splitting. Chemical Society Reviews, 38, 253–278. doi: 10.1039/B800489G
7. Bak T., Nowotny J., Rekas M., Sorrell C. (2002): Photo-electrochemical hydrogen generation from water using solar energy. Materials-related aspects. International Journal of Hydrogen Energy, 27, 991–1022. doi: 10.1016/S0360-3199(02)00022-8
8. Sakintuna B., Lamari-Darkrim F., Hirscher M. (2007): Metal hydride materials for solid hydrogen storage: A review. International Journal of Hydrogen Energy, 32, 1121–1140. doi: 10.1016/j.ijhydene.2006.11.022
9. Schlapbach L., Züttel (2001): Hydrogen-storage materials for mobile applications. Nature, 414, 353–358. doi: 10.1142/9789814317665_0038
10. Balat M. (2008): Potential importance of hydrogen as a future solution to environmental and transportation problems. International Journal of Hydrogen Energy, 33, 4013–4029. doi: 10.1016/j.ijhydene.2008.05.047
11. Wang M., Wang Z., Gong X., Guo Z. (2014): The intensification technologies to water electrolysis for hydrogen production - a review," Renewable and Sustainable Energy Reviews, 29, 573–588. doi: 10.1016/j.rser.2013.08.090
12. Fujishima A., Honda K. (1972): Electrochemical photolysis of water at a semiconductor electrode. Nature, 238, 37-38. doi: 10.1038/238037a0
13. Mavroides J., Kafalas J., Kolesar D. (1976): Photoelectrolysis of water in cells with $SrTiO_3$ anodes. Applied Physics Letters, 28, 241–243. doi: 10.1063/1.88723
14. Kay A., Cesar I., Graetzel M. (2006): New benchmark for water photooxidation by nanostructured Fe_2O_3 films. Journal of the American Chemical Society, 128, 15 714–15 721. doi: 10.1021/ja064380
15. Ye J., Zou Z., Oshikiri M., Matsushita A., Shimoda M., Imai M., Shishido T. (2002): A novel hydrogen-evolving photocatalyst $InVO_4$ active under visible light irradiation. Chemical Physics Letters, 356, 221–226. doi: 10.1016/S0009-2614(02)00254-3
16. Enache C., Lloyd D., Damen M., Schoonman J., van de Krol R. (2009): Photo-electrochemical properties of thin-film $InVO_4$ photoanodes: The role of deep donor states. The Journal of Physical Chemistry C, 113, 19 351–19 360. doi: 10.1021/jp9078663

17. Chen L., Alarcn-Llad E., Hettick M., Sharp I. D., Lin Y., Javey A., Ager J. W. (2013): Reactive sputtering of bismuth vanadate photoanodes for solar water splitting. The Journal of Physical Chemistry C, 117, 21 635– 21 642. doi: 10.1021/jp406019r
18. Wang M., Che Y., Niu C., Dang M., Dong D. (2013): Effective visible light-active boron and europium co-doped $BiVO_4$ synthesized by sol-gel method for photodegradion of methyl orange. Journal of Hazardous Materials, 262, 447–455. doi: 10.1016/j.jhazmat.2013.08.063
19. Liang Y., Tsubota T., Mooij L., van de Krol R. (2011): Highly improved quantum efficiencies for thin film $BiVO_4$ photoanodes. Journal of Physical Chemistry C, 115, 17 594–17 598. doi: 10.1021/jp203004v
20. Lin X., H.Li, Yu L., Zhao H., Yan Y., Liu C., Zhai H. (2013): Efficient removal rhodamine B over hydrothermally synthesized fishbone like $BiVO_4$. Materials Research Bulletin, 48, 4424–4429. doi: 10.1016/j.materresbull.2013.06.075
21. Hertkorn D., Elsenheimer H., Bruch R., Paul F., Mueller C., Hanemann T., Reinecke H. (2013): Thickness variation of electrophoretically deposited strontium titanate films for photoelectrochemical energy conversion. Journal of Applied Physics, 114(2). doi: 10.1063/1.4811817
22. Hamaker H. C. (1940): Formation of a deposit by electrophoresis. Transaction of Faraday Society, 35, 279–287. doi: 10.1039/TF9403500279
23. Walsh A., Yan Y., Huda M., Al-Jassim M., Wei S. H. (2009): Band edge electronic structure of $BiVO_4$: Elucidating the role of the Bi s and V d orbitals. Chemistry of Materials, 21, 547–551. doi: 10.1021/cm802894z
24. Yao W., Ye J. (2006): Photophysical and photocatalytic properties of $Ca_{1-x}Bi_xV_xMo_{1-x}$. The Journal of Physical Chemistry B, 110, 11 188–11 195. doi: 10.1021/jp0608729
25. Grimes S. R. C., Varghese O. (2008). Light, Water, Hydrogen: The Solar Generation of Hydrogen by Water Photoelectrolysis. Springer.
26. Abdi F., Savenije T., May M., Dam B., van de Krol R. (2013): The origin of slow carrier transport in $BiVO_4$ thin film photoanodes: A time-resolved microwave conductivity study. The Journal of Physical Chemistry Letters, 4, 2752–2757. doi: 10.1021/jz4013257
27. Kudo A., Omori K., Kato H. (1999): A novel aqueous process for preparation of crystal form-controlled and highly crystalline $BiVO_4$ powder from layered vanadates at room temperature and its photocatalytic and photophysical properties. Journal of the American Chemical Society, 121, 11 459–11 467. doi: 10.1021/ja992541y
28. Hertkorn D., Benkler M., Gleißner U., Buker F., Megnin C., Muller C., Hanemann T., Reinecke H. (2015): Morphology and oxygen vacancy investigation of strontium titanate-based photo electrochemical cells. Journal of Materials Science, 50, 40–48. doi: 10.1007/s10853-014-8563-y
29. Seabold J. A., Choi K. S. (2012): Efficient and stable photooxidation of water by a bismuth vanadate photoanode coupled with an iron oxyhydroxide oxygen evolution catalyst. Journal of the American Chemical Society, 134(4), 2186-2192. doi: 10.1021/ja209001d